Int J Thermophys (2010) 31:1719–1738
DOI 10.1007/s10765-010-0830-9

Progress in Noise Thermometry at 505 K and 693 K Using Quantized Voltage Noise Ratio Spectra

W. L. Tew · S. P. Benz · P. D. Dresselhaus · K. J. Coakley · H. Rogalla · D. R. White · J. R. Labenski

Received: 14 April 2010 / Accepted: 16 September 2010 / Published online: 6 October 2010

Abstract Technical advances and new results in noise thermometry at temperatures near the tin freezing point and the zinc freezing point using a quantized voltage noise source (QVNS) are reported. The temperatures are derived by comparing the power spectral density of QVNS synthesized noise with that of Johnson noise from a known resistance at both 505 K and 693 K. Reference noise is digitally synthesized so that the average power spectra of the QVNS match those of the thermal noise, resulting in ratios of power spectra close to unity in the low-frequency limit. Three-parameter models are used to account for differences in impedance-related time constants in the spectra. Direct comparison of noise temperatures to the International Temperature Scale of 1990 (ITS-90) is achieved in a comparison furnace with standard platinum resis-

W. L. Tew (✉)
Process Measurements Division (836), National Institute of Standards and Technology, Gaitherbsurg, MD 20899, USA
e-mail: wtew@nist.gov

S. P. Benz · P. D. Dresselhaus
Quantum Electrical Metrology Division (817), National Institute of Standards and Technology, Boulder, CO 80305, USA

K. J. Coakley
Statistical Engineering Division (898), National Institute of Standards and Technology, Boulder, CO, USA

H. Rogalla
University of Twente, Enschede, The Netherlands

D. R. White
Measurement Standards Laboratory of New Zealand, P.O. Box 31310, Lower Hutt 5040, New Zealand

J. R. Labenski
BAE Systems, Arlington, VA, USA

tance thermometers. The observed noise temperatures determined by operating the noise thermometer in both absolute and relative modes, and related statistics together with estimated uncertainties are reported. The relative noise thermometry results are combined with results from other thermodynamic determinations at temperatures near the tin freezing point to calculate a value of $T - T_{90} = +4(18)$ mK for temperatures near the zinc freezing point. These latest results achieve a lower uncertainty than that of our earlier efforts. The present value of $T - T_{90}$ is compared to other published determinations from noise thermometry and other methods.

Keywords ITS-90 · Johnson noise thermometry · Synthesized noise · Temperature · Zinc freezing point

1 Introduction

Recent technological improvements have advanced Johnson noise thermometry (JNT) using quantized voltage noise sources (QVNS) [1]. These advances have been applied to our continuing efforts to determine thermodynamic temperatures T versus the International Temperature Scale of 1990 (ITS-90), T_{90} in the range from 505 K to 693 K. In this article, we report on our most recent spectral noise-ratio data for these temperatures and compare the results to those obtained in our previous noise thermometry work [2,3].

The power spectral density of voltage fluctuations, S_R, in a metal conductor of resistance R at temperature T, in the low-frequency high-temperature limit, is given by the Nyquist approximation,

$$S_R = 4k_B TR, \tag{1}$$

where k_B is Boltzmann's constant. This noise is random, Gaussian, and remains white (frequency-independent) out to frequencies $\sim k_B T/h = 10$ THz at 505 K, where quantum corrections become important. In practice, such high cutoffs are never directly observable due to the limiting frequency response associated with non-intrinsic time constants that are many orders of magnitude larger and are governed by the unavoidable parasitic impedances of real macroscopic circuits and cables. In any case, the leading correction term to Eq. 1 is $(hf/(k_B T))^2/12$ which means the Nyquist approximation would be expected to remain valid at 1 MHz and 500 K to within 1×10^{-15}.

Digitally synthesized noise waveforms can now be created via pulse-biased Josephson junction arrays forming a QVNS [4]. The power spectral density S_Q of a QVNS array of N_J junctions operating at a sampling frequency f_s and a repetition rate f_1 is given by

$$S_Q = \frac{D^2 N_J^2 f_s^2}{K_J^2 f_1}, \tag{2}$$

where K_J is the Josephson constant and D is a dimensionless parameter calculated from the digital synthesis [5]. This noise is non-random (i.e., deterministic) [6], approxi-

mately Gaussian in the fluctuating (i.e., time-dependent) voltage amplitudes, and constructed to be of a constant average spectral density out to some maximum frequency $f_{\max}$.

If the ratio S_R/S_Q can be accurately measured, then it is possible to determine an absolute noise temperature T by

$$T = \frac{\langle S_R \rangle}{\langle S_Q \rangle} \frac{f_1 K_J^2}{4 k_B R D^2 f_s^2 N_J^2}. \tag{3}$$

This is the basis for JNT using a QVNS in the absolute mode [7].

In absolute mode, the noise signals are subject to differential filtering whenever the line and source impedances for the two sources are unmatched [8]. Imperfect impedance matching necessitates applying a frequency-dependent correction, where the factor $\langle S_R \rangle / \langle S_Q \rangle$ in Eq. 3 is taken in the low frequency limit. In the lumped-impedance-parameter approximation, it is straightforward to show that the frequency correction has the form,

$$\frac{\langle S_R \rangle}{\langle S_Q \rangle} \cong \frac{\langle S_R \rangle}{\langle S_Q \rangle}\bigg|_0 \sum_{j=1} \left[1 + \left(\tau_{Qj}^j - \tau_{Rj}^j\right) \omega^j\right], \tag{4}$$

where the τ_Q and τ_R are effective time constants associated with source, line, and input impedances for each of the two input networks with subscripts "R" for the resistor and "Q" for the QVNS. The R and Q input networks are primarily composed of: source/series resistances $R(T)$, R_Q; series inductances L_R, L_Q; and shunt capacitances C_R, C_Q [9]. Ratio spectra are predominately quadratic below 1 MHz, and the τ_{Q2} and τ_{R2} constants are dominated by RC and LC couplings. There are also small 4th-degree frequency terms, where the τ_{Q4} and τ_{R4} constants are dominated by LC couplings [10]. The corresponding source impedances, however, do not couple in identical ways in the two networks. The QVNS has practically zero source impedance which decouples the two halves of that input network and halves the effective shunt capacitance when compared to the analogous terms in the R network [8]. In practice, the frequency-dependent correction is accomplished by statistical fitting of a simple polynomial function of frequency to the data, such as $\langle S_R \rangle / \langle S_Q \rangle = a_0 + a_1 f + a_2 f^2 + a_3 f^3 + a_4 f^4$, where the odd terms can be ignored when dielectric losses are small [9].

If noise-power measurements are performed at two different temperatures, T_1 and T_2, the ratio of the power spectra can be used to determine the temperature T_2 in terms of T_1, which may be any convenient reference temperature. In this relative mode, T_2 is given by

$$T_2 = \frac{\langle S_{R,T_2} \rangle}{\langle S_{Q_2} \rangle} \frac{\langle S_{Q_1} \rangle}{\langle S_{R,T_1} \rangle} \frac{D_1^2}{D_2^2} \frac{R(T_1)}{R(T_2)} T_1. \tag{5}$$

The ratio T_2/T_1, while insensitive to many systematic errors that affect the absolute measurements, is subject to frequency response effects due to the time

constants $\tau_{\mathrm{R}\,j}(T)$ which are normally temperature-dependent [11], and sometimes time-dependent. By extension of the same parameterization of time constants of Eq. 4, we then have

$$\frac{\langle S_{\mathrm{R}T_2}\rangle}{\langle S_{\mathrm{Q}_2}\rangle}\frac{\langle S_{\mathrm{Q}_1}\rangle}{\langle S_{\mathrm{R}T_1}\rangle} \cong \frac{\langle S_{\mathrm{R}T_2}\rangle}{\langle S_{\mathrm{Q}_2}\rangle}\bigg|_0 \frac{\langle S_{\mathrm{Q}_1}\rangle}{\langle S_{\mathrm{R}T_1}\rangle}\bigg|_0 \sum_{j=1}\left[1+\left(\tau^j_{\mathrm{R},\,j}(T_1)-\tau^j_{\mathrm{R},\,j}(T_2)\right)\omega^j\right] \tag{6}$$

All terms involving $\tau_{\mathrm{Q},\,j}$ are cancelled in the relative mode, provided that all QVNS input network impedances are stationary. The same approach to the parameterization of the correction model also applies in the relative mode case, but the correction coefficients $a_j\,(j>0)$ are usually much smaller than in the absolute case.

2 Experimental Systems

The National Institute of Standards and Technology (NIST) maintains two operational JNT systems utilizing QVNS references. The first JNT system is located at NIST in Boulder, CO and is optimized for operation at 273.16 K in the absolute mode with a fixed 100.0 Ω source resistance [14]. The second system is located at NIST in Gaithersburg, MD and operates primarily in the relative mode in the range of 505 K to 930 K with variable source impedances [3]. While the majority of our recent publications have described results obtained in the Boulder JNT system, this article describes results obtained in the Gaithersburg system. Much of the electronics and QVNS-specific hardware in the two systems are similar, but certain differences do exist and these will be noted where they affect specific measurement issues.

The experimental setup as shown in Fig. 1 consists of: a QVNS system, a high-temperature-resistance probe, a digital-noise-voltage correlator, and a vacuum-comparison furnace system. All the systems are housed in an electromagnetically shielded facility in Gaithersburg. Similar systems were in place at the Gaithersburg facility for our earlier measurements as reported in 2008 [3], but several important changes and improvements have taken place since that work was completed.

2.1 QVNS

The QVNS used in the Gaithersburg JNT system is based on the same basic Josephson-junction technology as used in Boulder JNT systems [13]. The specific system described here is based on a dual array of ten junctions, each with critical currents of $I_{\mathrm{c}}(4.2\mathrm{K}) \cong 4.8$ mA and four (two for each channel) $R_{\mathrm{Q}} = 97\ \Omega$ on-chip series resistor terminations. This QVNS circuit has significantly fewer junctions than used in the 2008 work, and this necessitates new modulator bit patterns, but the basic current-pulse biasing scheme and $f_{\mathrm{s}} = 10$ GHz clock are unchanged.

An important distinction for the Gaithersburg QVNS is the use of an older model of a semiconductor bit-stream generator with less memory capacity, which in practice limits the pattern repetition rate to $f_1 \sim 1.6$ kHz. The more-advanced Boulder system can produce patterns with four times lower repetition rates. Another difference lies

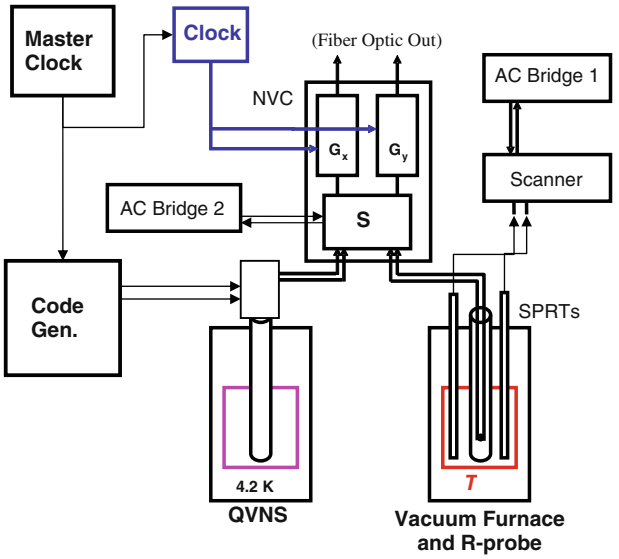

Fig. 1 Functional diagram of the NIST Gaithersburg JNT measurement system: *NVC* noise voltage correlator electronics; *S* switching network, G_x, G_y analog gain blocks and digitizers, *Code Gen.* bit stream generator with 10 GHz clock (see text)

in the construction of the cryo-probe output cables, which in the Boulder system, are configured with a lower shunt capacitance over the ∼1 m length of the probe. The Gaithersburg QVNS probe is not tuned in this way and, hence, presents a larger shunt capacitance to the amplifier inputs than is present in the resistance probe. This cable configuration is essentially the same as that used in our 2008 work. The 97 Ω terminations, however, are almost double the resistance of those used in 2008, and this serves to almost double the *RC* time constant defining the bandwidth of the source.

The binary patterns of pulses used to generate the pseudo-noise waveforms for each temperature are computed from a delta-sigma algorithm starting from the desired spectral distribution of tones and their specific randomized phase relationships [4]. A single-base spectrum with a fixed random phase distribution is used to generate all the necessary QVNS spectra by varying only the amplitudes of the tones to match the spectral density for each *RT* product of the resistance probe. We used the same, odd-only, harmonic series with a fundamental frequency $f_1 = 1.589$ kHz and $f_{\max} = 8$ MHz that we used in our 2008 experiments.

2.2 Resistance Probe and Measurements

The quartz-sheathed resistance probe is of an identical design to that used in 2008, but has been rebuilt using new silver lead wire and different Pt-8 %W alloy resistors. The same quartz insulators are used, but these have been inverted so that the hot and cold ends are switched. The use of the same alloy wire in the new resistors (also trimmed to 100 Ω at 273.15 K) results in $R(505\ \text{K}) \cong 107\ \Omega$ and $R(693\ \text{K}) \cong 113\ \Omega$ with a

temperature coefficient of resistance $\alpha_R \cong 290\ \mu\Omega \cdot \Omega^{-1} \cdot K^{-1}$. A small modification of the probe was made to accommodate purging of the interior with argon gas. The resistors remained very stable under thermal cycling in the temperature range under investigation.

The resistance of the probe was measured, using a two-terminal-pair AC resistance bridge operating at 90 Hz, and at intervals of ∼2000 s during data acquisition. The reference resistor was a calibrated 100 Ω non-inductive standard with a low AC-DC difference. The bridge had a resolution of $1\ \mu\Omega \cdot \Omega^{-1}$ and exhibited rms noise on the same level. We assigned a combined ($k = 1$) measurement uncertainty of $2\ \mu\Omega \cdot \Omega^{-1}$ for the absolute resistance.

2.3 Noise Voltage Correlator Electronics

The two-analog channel sections of the noise voltage correlator (referred to as the "correlator" from this point forward) electronics have been replaced with an improved version having approximately 40 dB additional common mode-rejection ratio [14]. The new design has a similar low-noise preamplifier with an equivalent input noise of $1.4\ nV \cdot Hz^{-1/2}$ which is DC coupled to the noise sources, while the old version used in our 2008 work was AC coupled.

Filtering in the new design is accomplished via an 11-pole passive low-pass filter with a 650 kHz 3 dB cut-off frequency. This replaces both a 2 MHz 3 dB anti-alias active filter stage and the 200 kHz 3 dB digital filter, which had been used in our previous work in Gaithersburg (and also in the Boulder JNT system prior to ∼2006). These new passive filters are highly stable and define the usable bandwidth of the system. They are utilized in conjunction with the new amplifier circuits in a buffered configuration as described in the recent article by Qu et al. [14] (Version "B" in Fig. 1 of [14]).

The analog-to-digital converter (ADC) is the same 14-bit model as described previously [15] that digitizes the amplifier output at 50 MHz, and is followed by field programmable gate arrays (FPGAs) for additional processing. These FPGAs previously implemented the 200 kHz digital filter, but that function has been disabled in this work so that the only function of the FPGAs now is to accumulate and re-sample the data at 2.083 MHz and 21 bits for optical encoding. The data processing from the optical stream, including Fourier transform and correlation spectra computations, is essentially the same as described in our prior studies [15].

The inputs to the correlator are switched between the two sources "R" and "Q" every 100 s. The printed-circuit board previously used for switching between sources has been replaced for this work with a new board and new relays, but is of the same design as used in our 2008 work. After publication of our 2008 work, it became clear that the old circuit board was irreversibly damaged by moisture intrusion and that this damage was most likely responsible for the instabilities (primarily drift) and dielectric losses encountered in that experiment [3].

2.4 Comparison Furnace System

The vacuum comparison furnace is the same three-zone system as described in our prior JNT work [2]. For the present work, we use two new standard platinum resistance

thermometers (SPRTs) calibrated at NIST over the ITS-90 subrange between the water triple point (WTP) and aluminum freezing point (273.16 K to 933.473 K) [12]. This includes calibration points at the tin freezing point (Sn FP, $T_{90} \equiv 505.078$ K) and the zinc freezing point (Zn FP, $T_{90} \equiv 692.677$ K).

The furnace temperature was continuously measured via the SPRTs, along with other environmental temperatures, at approximately 10 min cycles. This is accomplished via a second two-terminal-pair AC resistance bridge also operating at 90 Hz with a calibrated 25 Ω non-inductive standard reference resistor. The bridge has a resolution of 25 μΩ (0.25 mK) and exhibited rms noise on the same level.

The furnace utilizes two active control zones: an outer "guard" zone and an inner "shell" zone. A third innermost zone, the "core," passively equilibrates through a weak thermal coupling to the shell and contains the SPRT thermowells and the central thermowell for the noise probe. The furnace core exhibits an rms stability of 0.5 mK at 505 K and typically 2 mK to 3 mK at 694 K depending on the room-temperature control stability.

3 Results

The data described here were obtained over a three-month period starting in October 2009 and ending in January 2010. Table 1 summarizes the key parameters for each of the four basic data groups at three separate temperatures. Each data group is a collection of five to seven separate runs, most of which are between 12 h and 16 h in duration. The data groups, "Oct 505" and "Jan 505," were obtained at temperatures within 0.25 K above the Sn FP, which served as our reference temperature. The data groups, "Nov 694" and "Dec 692," were obtained at temperatures 1.26 K above and 0.19 K below the Zn FP, respectively.

3.1 Raw Spectra

The raw spectra for a given run consist of the two channels: power spectra and one cross spectrum each comprising over 1×10^6 bins of 0.993 Hz width, for both the QVNS and the resistance probe. The cross spectra are a measure of the power of the noise from the resistor or the QVNS only, while the power spectra for each channel

Table 1 Data summary

Data group ID	Dates	Total time duration (h)	Average temperature (K)
Oct 505	22 Oct to 30 Oct 09	82	505.27
Nov 694	16 Nov to 20 Nov	62	693.94
Dec 692	30 Nov and 16 Dec to 23 Dec	61	692.49
Jan 505	5 Jan to 18 Jan 2010	87	505.30

Dates listed are the range over which data were obtained, but do not necessarily correspond to continuous time intervals

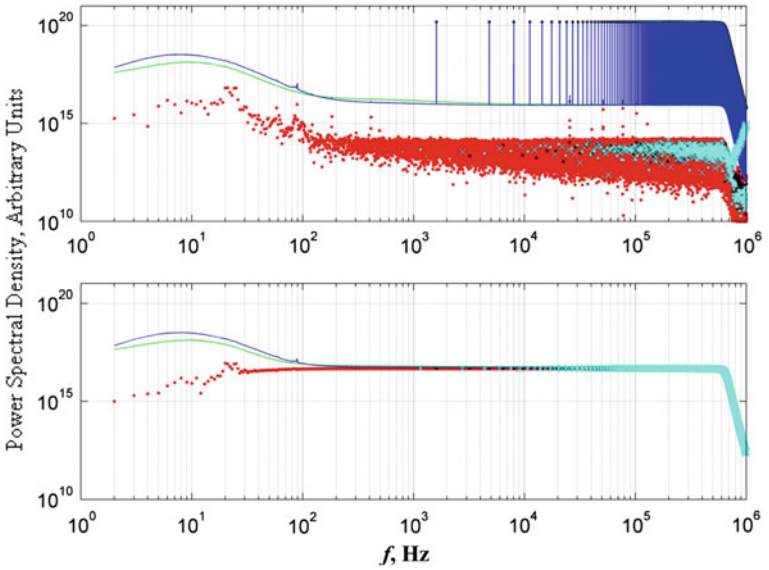

Fig. 2 Raw QVNS (*top*) and R-probe (*bottom*) spectra with ∼1 Hz wide bins. Both noise power spectra for each amplifier channel appear along with the cross-correlated spectrum for the two sources. Locations of each QVNS harmonic (both odd and even) appear as *black dots* and the aliased tone locations appear as *light blue dots* and × *symbols* (Color figure online)

of the correlator are a measure of the noise sources plus the uncorrelated noise from the amplifiers. An example of the raw spectra is shown in Fig. 2.

3.2 Ratio Spectra for Absolute Mode

In the absolute mode, power-spectra ratios are formed by re-binning the raw cross-spectra data from the resistor probe as averages of 3200 of the 0.993 Hz bins centered at the location of each QVNS tone starting with the 3rd harmonic at 4.768 kHz. The QVNS cross spectra are then re-binned in the same way by averaging the central tone with all other bins within a 3200 bin interval out to and including the 375th harmonic centered at 596 kHz. These re-binned spectra of 187 bins each, are then averaged over the duration of the run. The two averaged spectra, for each of the "R" and "Q" sources, are then used to form a "ratio spectrum" $\langle S_R \rangle / \langle S_Q \rangle$ for each run through bin-by-bin division in 3.179 kHz wide bins.

An average ITS-90 temperature, T_{90}, is calculated for each run from SPRT data along with an average resistance $R(T)$ of the R-probe. These data are used to calculate $S_{R\text{-}90} \equiv 4k_B T_{90} R(T)$ and $X_{90} \equiv S_{R\text{-}90}/S_Q$. By design, X_{90} is within 0.2 % of unity, but may vary slightly from one run to the next within a data group due to drift in the furnace controls. In order to combine various individual runs into one grand averaged spectrum for an entire data group, we normalized all the ratio spectra $S \rightarrow S'$ to be unity when $T = T_{90}$. The normalization is accomplished by a simple shift of the origin or $\langle S'_R \rangle / \langle S'_Q \rangle = \langle S_R \rangle / \langle S_Q \rangle - X_{90} + 1$. Examples of such normalized absolute ratio spectra for two data groups (Oct 505 and Nov 694) are shown in Fig. 3.

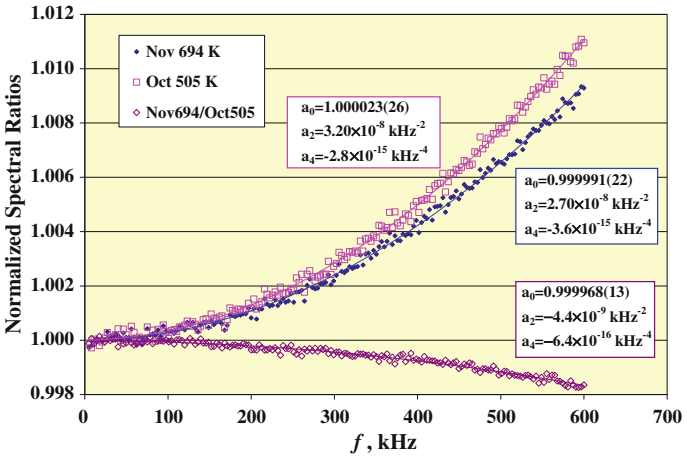

Fig. 3 Absolute-ratio spectra for the Nov 694 and the Oct 505 data groups and the relative ratio spectrum derived by their combination. Fit parameters are shown for the 3PE correction model

Table 2 3PE fitting parameters and statistical uncertainties for the absolute spectra

Data group ID	a_0	a_2 (kHz^{-2})	a_4 (kHz^{-4})
Oct 505	1.000 023 (26)	3.16 (0.04) $\times 10^{-8}$	-2.8 (1.3) $\times 10^{-15}$
Nov 694	0.999 991 (22)	2.72 (0.04) $\times 10^{-8}$	-3.6 (1.2) $\times 10^{-15}$
Dec 692	0.999 994 (23)	2.74 (0.04) $\times 10^{-8}$	-4.0 (1.2) $\times 10^{-15}$
Jan 505	1.000 012 (26)	3.26 (0.05) $\times 10^{-8}$	-4.4 (1.4) $\times 10^{-15}$

The normalized absolute ratio spectra for the four data groups are fitted by a three-parameter even-degree (3PE) model $a_0 + a_2 f^2 + a_4 f^4$ from 4.8 kHz to 596 kHz. The fitted parameters and their statistical uncertainties are given in Table 2. The statistical uncertainties for the a_0 parameters in the four fitted spectra vary between 22 $\mu\mathrm{K}\cdot\mathrm{K}^{-1}$ and 26 $\mu\mathrm{K}\cdot\mathrm{K}^{-1}$. These are approximately three times greater uncertainties than what would be expected in this model, averaging time, and bandwidth [6]. This statistical inflation is caused by distortion in the QVNS waveforms from small non-linear effects in the amplifiers [14]. Distortion was also present in our 2008 work; however, in the present data the low-frequency distortion products are significantly smaller.

Other correction models, which include odd-degree terms may also be used for the absolute-mode data to account for small dielectric losses. Given the degree of distortion present in these data, and the relatively small magnitude of the odd-degree coefficients, however, it is not possible to distinguish the preferred model from statistical criteria alone. Moreover, when odd-degree terms are allowed, the fitting process often results in predictions for the a_1 parameter which are unphysical in magnitude and/or sign. This situation necessitates the adoption of an *a priori* approach to the estimation of odd-degree terms, and this process is discussed in Sect. 4.

Table 3 3PE correction model parameters for the relative spectra

Data group combination	a_0	a_2 (kHz^{-2})	a_4 (kHz^{-4})
Nov 694/Oct 505	0.999 968 (13)	$-4.37\,(0.23) \times 10^{-9}$	$-6.4\,(7.1) \times 10^{-16}$
Nov 694/Jan 505	0.999 979 (13)	$-5.42\,(0.22) \times 10^{-9}$	$9.9\,(6.7) \times 10^{-16}$
Dec 692/Oct 505	0.999 971 (16)	$-4.18\,(0.28) \times 10^{-9}$	$-1.08\,(0.86) \times 10^{-15}$
Dec 692/Jan 505	0.999 982 (13)	$-5.24\,(0.23) \times 10^{-9}$	$5.5\,(7.0) \times 10^{-16}$

3.3 Ratio Spectra for Relative Mode

The required ratio spectra for the relative mode are derived from a pair of absolute-mode ratio spectra as indicated by Eq. 5. The relative spectra are computed from bin-by-bin quotients in the four possible combinations of the data groups keeping the 505 K ratio spectra in the denominator. An example of a relative-mode ratio spectrum is shown as the lower trace in Fig. 2 for the Nov 694 and the Oct 505 data groups. When the same 3PE model is fitted to the relative ratio spectra, the statistical uncertainties in the a_0 parameters are reduced to values between 13 $\mu\mathrm{K}\cdot\mathrm{K}^{-1}$ and 16 $\mu\mathrm{K}\cdot\mathrm{K}^{-1}$ when compared to $\sim$34 $\mu\mathrm{K}\cdot\mathrm{K}^{-1}$, which would be expected on the basis of combining two uncorrelated absolute ratio spectra. This reduction in uncertainty occurs because the distortion products in the QVNS spectra are mostly stationary and, hence, correlated from one data group to the next. Table 3 summarizes the 3PE fits for the relative spectra.

Another feature of the 3PE fits of the relative-mode ratio spectra is the weak statistical significance of the a_4 term. This is to be expected given that most *LC* coupling terms should be both temperature-independent and stationary so that $\tau_{\mathrm{R},4}(694\,\mathrm{K}) - \tau_{\mathrm{R},4}(505\,\mathrm{K}) \cong 0$. The model estimates for the relative-mode spectra, however, appear to be consistent with the apparent negative drift in time of the a_4 coefficient as shown in the absolute-mode spectra. The statistical significance of this term is therefore slightly higher for the two relative-mode spectra combinations (Nov 694/Jan 505 and Dec 692/Oct 505), which are separated by two months in time rather than only one month.

In our previous work at 693 K, we utilized the three-parameter correction model $a_0 + a_1 f + a_2 f^2$ out to frequencies of 450 kHz. This three-parameter model, with both odd and even (i.e., "all," or 3PA) parameters, was necessary due to the existence of a variable dielectric loss in the fiberglass insulation of the switch card used during that experiment. While the dielectric losses are much smaller in the present work, they may not necessarily be negligible. In fact, the relative contribution of the linear term (e.g., a_1/a_2) is expected to be greater in the relative-mode spectra than the absolute-mode spectra, so we also calculate 3PA fits for the relative-mode spectra and these are shown in Table 4. In this case, the values for the a_1 coefficients predicted by the fitting process are within the bounds predicted by an *a priori* lumped-parameter impedance model (see Sect. 4.1) in three of the four relative ratio spectra.

The statistical uncertainty $s(a_0)$ in the in a_0 parameter, as shown in Tables 2, 3, and 4 is primarily determined by either random components or distortion products which may be present in the spectra, whichever is dominant. In general, the addition of more fit parameters will also increase $s(a_0)$, but the degree of increase depends on

Table 4 3PA correction model parameters for the relative spectra

Data group combination	a_0	a_1 (kHz^{-1})	a_2 (kHz^{-2})
Nov 694/Oct 505	0.999 984 (22)	$-7.64\,(0.17) \times 10^{-8}$	$-4.44\,(0.27) \times 10^{-9}$
Nov 694/Jan 505	0.999 966 (20)	$1.63\,(0.16) \times 10^{-8}$	$-5.14\,(0.25) \times 10^{-9}$
Dec 692/Oct 505	1.000 003 (26)	$-1.7\,(2.0) \times 10^{-7}$	$-4.25\,(0.32) \times 10^{-9}$
Dec 692/Jan 505	0.999 985 (21)	$-8.2\,(16) \times 10^{-8}$	$-4.94\,(0.26) \times 10^{-9}$

the functional form of the additional terms. For the absolute spectra, the addition of the quartic term with a 3rd parameter a_4 introduces only a relatively minor increase in $s(a_0)$ when compared to that which would occur for a simple two-parameter quadratic model. This is because a_0 is most sensitive to the low frequency data and a_4 is only sensitive to the highest frequency data, so the two parameters have a relatively small covariance. The values for $s(a_0)$ for the absolute data in Table 2 are almost entirely due to distortional variance and very little due to the addition of the third parameter.

On the other hand, our relative mode data exhibit much lower distortion effects, and the statistics are closer to what would be expected for random correlations for the finite sample times. There are noticeable differences in $s(a_0)$, however, between the 3PE and 3PA fits in Tables 3 and 4. In the 3PA case, the linear parameter a_1 is equally sensitive to both ends of the ratio spectrum and a significant covariance exists between a_1 and a_0. The addition of the linear term causes the uncertainty in a_0 to increase by approximately a factor of two when compared to that from a simple two-parameter quadratic model alone or even the 3PE model. So in the relative spectra, the form of the correction model is an important factor in determining $s(a_0)$.

4 Discussion and Uncertainties

In some respects, this work is a replication of our earlier 2008 report [3] in that similar methods and equipment have been used. On the other hand, the present work is significantly different in several critical aspects due to improvements made since the completion of the earlier work.

Foremost, among these differences between this and the earlier work is the improved long-term stability of the system in the absolute mode. In our previous work, it was necessary to apply a 6 $\mu K \cdot K^{-1} \cdot day^{-1}$ correction in the relative mode to account for an observed systematic drift. Even though an allowance for this correction was made in the uncertainty budget, we still considered this to be a central weakness in that result since, at the time, the origin of the effect was not understood. A drift correction was not necessary in the present work even though the duration of the experiment was approximately four times longer. Replacing the defective circuit board eliminated the most problematic drift and reduced the observed dielectric loss to manageable levels. Small changes were observed, however, in the 505 K absolute ratio spectra during the three-month time interval, but these were not significant at low frequencies. The details of these and other sources of uncertainty are discussed below.

4.1 Correction Models

In this work, we have utilized both a 3PE model, $a_0 + a_2 f^2 + a_4 f^4$, and a 3PA model, $a_0 + a_1 f + a_2 f^2$, with an upper-range limit of 596 kHz. The absence of a linear term in the 3PE model is significant because it improves the statistical uncertainty for the a_0 parameter despite having the same number of model parameters overall. However, there is no clear way to differentiate these two physically plausible models from one another based on statistical considerations alone. Furthermore, other alternative models with more parameters cannot necessarily be ruled out based on statistics. This is particularly true in the distortion-limited absolute-mode spectra, and it creates a small degree of ambiguity in the results that we account for with an uncertainty component u_{cm}.

Fortunately, bounds can be placed on the physically realistic values of any possible a_1 terms through simple lumped-parameter estimations of these terms and knowledge of dielectric losses in the most suspect insulators of the input networks. These are the new switch cards, again made from standard epoxy-fiberboard (FR4), and the hot sections of quartz insulators used in the R-probe. For the absolute-mode spectra, we estimate the sign and magnitude of any linear frequency correction term $a_{1-\mathrm{Est}}$ as

$$a_{1-\mathrm{Est}} \approx 2\pi \left\{ \left(2R_{\mathrm{Q}} - [2 - T_{\mathrm{FR4}}/T]\, R(T)\right) C_{\mathrm{FR4}} \tan\delta_{\mathrm{FR4}} - \left[2 - T_{\mathrm{qz}}/T\right] R(T)\, C_{\mathrm{qz}} \tan\delta_{\mathrm{qz}} \right\}, \tag{7}$$

where R_{Q} is the single-end series termination resistance of the QVNS probe; $R(T)$ is the differential resistance of the R-probe; C_{FR4} is the effective shunt capacitance for the FR4 dielectric in the switch card traces (assumed to be equal for R and Q inputs); $\tan\delta_{\mathrm{FR4}}$ is the associated loss tangent for the FR4 dielectric; T_{FR4} is the switch-card temperature; and C_{qz}, $\tan\delta_{\mathrm{qz}}$, and T_{qz} are the effective shunt capacitance, loss tangent, and temperature, respectively, for the hot sections of the quartz insulators in the R-probe. Equation 7 is a superposition of the noise from R attenuated by the RC-filter and the noise of the dielectrics similarly attenuated. Only those dielectric losses in the R-network contribute correlated noise since the two halves of the Q-network are decoupled by the QVNS source. Given realistic values for all of the physical parameters, we estimate $a_{1-\mathrm{Est}}(505) \approx +6(4) \times 10^{-8}\,\mathrm{kHz}^{-1}$ and $a_{1-\mathrm{Est}}(694) \approx -5.4(7.7) \times 10^{-8}\,\mathrm{kHz}^{-1}$ for the absolute-mode spectra. These *a priori* predictions are small in magnitude, but highly uncertain. Attempts to fit the absolute spectra to a model with a linear coefficient as a free parameter results in fitted values for a_1 outside of the range of these *a priori* estimates (i.e., unphysical) and of marginal statistical significance.

As an alternative to fitting the a_1 parameter, the effects of small dielectric losses on the measured absolute noise temperatures can be accessed by including a linear frequency term with fixed a_1 and refitting the data to the 4th-degree polynomial ($a_3 = 0$). We have used a Monte-Carlo simulation to sample values of a_1 from a uniform distribution within the range predicted by Eq. 7 for assessing the correlation between fitted values of a_0 and assumed values of a_1 for the absolute-mode data. The results, as shown in Table 5, yield a linear dependence between the fitted values of a_0 and the assumed value of a_1 with a negative slope $\Delta a_0/\Delta a_1$. When these linear functions are

Table 5 Summary of *a priori* dielectric loss corrections to the 3PE model for absolute-mode data

	Oct 505	Nov 694	Dec 692	Jan 505
$a_{1-\mathrm{Est}}$ (kHz^{-1})	$+6(4) \times 10^{-8}$	$-5.4(7.7) \times 10^{-8}$	$-5.4(7.7) \times 10^{-8}$	$+6(4) \times 10^{-8}$
$\Delta a_0/\Delta a_1$ (kHz)	-6.9×10^{7}	-7.3×10^{7}	-7.1×10^{7}	-7.1×10^{7}
Δa_0 ($\mu\mathrm{K} \cdot \mathrm{K}^{-1}$)	−4.2	3.9	3.8	−4.3
Corrected $[a_0 - 1]$ ($\mu\mathrm{K} \cdot \mathrm{K}^{-1}$)	18.8	−5.1	−2.2	7.7

applied as corrections to the 3PE model results, the a_0 values for the 505 K data are shifted down by $\sim$4 $\mu\mathrm{K} \cdot \mathrm{K}^{-1}$ and the 694 K data are shifted up by approximately the same amount. The uncertainties in making these corrections are $\sim$3 $\mu\mathrm{K} \cdot \mathrm{K}^{-1}$ and 5.6 $\mu\mathrm{K} \cdot \mathrm{K}^{-1}$, respectively.

Another implicit assumption being made in the approximations leading to Eq. 7 is that the loss tangents are frequency-independent. This is not always the case, but the degree of frequency dependence observed in these insulators is normally very weak over the frequencies of interest here. Given the uncertain nature of these corrections, together with the lack of quantitative estimates on the size of a_3 (which we ignore in this work) and the related model ambiguities, we assign an overall correction model uncertainty of $u_{\mathrm{cm}} = 20\ \mu\mathrm{K} \cdot \mathrm{K}^{-1}$ for the absolute-mode data.

The estimate for the a_1 parameter for the relative-mode spectra is given by the difference of the absolute-mode estimated coefficients $a_{1-\mathrm{Est}}(694)$ and $a_{1-\mathrm{Est}}(505)$, or $a_{1-\mathrm{Est}}(694/505) \approx -1.1(0.4) \times 10^{-7}\,\mathrm{kHz}^{-1}$. Three of the four 3PA fits shown in Table 4 yield fitted values of a_1 which are within the bounds of this estimate (i.e., $a_{1-\mathrm{Est}} \leq a_1 \pm u(a_1) \leq 0$). In light of these observations, we view the 3PA fits to be the more physically correct model appropriate for the relative-mode ratio spectra of this work. When averaged over all spectral ratio combinations, the difference between the a_0 parameter as derived by the 3PE and 3PA fits is only $\sim$10 $\mu\mathrm{K} \cdot \mathrm{K}^{-1}$, which is within the statistical uncertainties of either model's estimates. We assign an additional Type B uncertainty $u_{\mathrm{cm}} = 10\ \mu\mathrm{K} \cdot \mathrm{K}^{-1}$ to account for the remaining small degree of ambiguity for the relative-spectra correction model.

4.2 Non-Linearity and Distortion

The presence of distortion is evident in the absolute-mode spectra and, as already discussed in Sect. 3, this distortion is the dominant source of dispersion limiting the statistical uncertainty for the correction model parameters. The correlation coefficients for pairs of residuals of the 3PE fits to the absolute-mode spectra vary between approximately 0.78 and 0.88 (see Table 6), which is consistent with the observation that the majority of the distortion remained stationary throughout the experiment.

Table 6 Correlation coefficients for the 3PE residuals of absolute spectra pairs

Data group pair	Nov 694, Oct 505	Nov 694, Jan 505	Dec 692, Jan 505	Dec 692, Oct 505	Nov 694, Dec 692	Oct 505, Jan 505
$C_{1,2}$	0.852	0.879	0.867	0.781	0.838	0.871

Some distortion, however, was of a variable nature. The degree to which the variable distortion influences the correction models is most readily estimated by comparing the results for the 3PE fits of the Oct 505 and the Jan 505 absolute spectra. Since the a_0 parameters differ by only 11 $\mu K \cdot K^{-1}$ with 26 $\mu K \cdot K^{-1}$ statistics, we conclude that any bias effect from variable distortion is unresolvable. Hence, we allow a small uncertainty component of 11 $\mu K \cdot K^{-1}$ in the absolute spectra and 3.7 $\mu K \cdot K^{-1}$ in the relative spectra for the possible bias effects (i.e., non-statistical) due to distortion, both variable and stationary.

4.3 EMI

The presence of narrow band EMI harmonics, starting at ∼26 kHz, is evident in the QVNS raw spectra as shown in Fig. 2. This EMI remained relatively stationary during the entire duration of the experiment. Similar EMI could also be present in the R spectra, but if comparable in amplitude it would remain unresolved when compared to the much higher continuous correlated noise spectral density of the R-probe. Even if this EMI was only present in the QVNS spectra, the net effect on the ratio spectra would still be negligible since it is limited to only a few 0.993 Hz frequency bins and more than −40 dBc in relative magnitude for the four-to-five resolvable harmonics.

As indicated in Sect. 3.2, the re-binning method employed in this work averages all the data over 3200 of the 0.993 Hz bins surrounding any given QVNS tone. This has been referred to as a "Bin" analysis in prior works. This is in distinction to the "Peak"-analysis method used for computing results in our prior 2008 work, which ignored the content of all other bins that did not contain the QVNS tone. In this work, we compared spectra from individual runs using the "Bin"- and "Peak"-analysis methods, and in all cases, the results differed by less than the statistical precision of either result and were often $<\sim 10\ \mu K \cdot K^{-1}$. This difference is a measure of the effects of EMI in the QVNS spectra, the presence of aliased tones, and the presence of distortion products.

Low-level EMI that could be present in the R-spectra alone is not readily detectable. If such EMI contamination did exist and was stationary, it would affect the results of the absolute-mode spectra, but cancel in the relative-mode spectra. Non-stationary EMI would be expected to affect the relative-mode results slightly more than in the absolute-mode results. In this work the results from the two modes at 693 K agree to well within the statistical bounds. Under the assumption that equal, but uncorrelated, amounts of stationary and non-stationary EMI are corrupting all the absolute spectra resulting in errors of $\sim 10\ \mu K \cdot K^{-1}$ each, the net effect on both the absolute spectra and the relative spectra would be a probable error of 14 $\mu K \cdot K^{-1}$. We therefore assign a Type B EMI uncertainty component of $u_{EMI} = 14\ \mu K \cdot K^{-1}$ for both the absolute mode and the relative mode results.

4.4 Stability

The system is designed to account for most forms of instability or drift. Drift in the amplifier gains is automatically canceled by alternate switching of the inputs. Drift in the input network impedances is accounted for by grouping the data into contig-

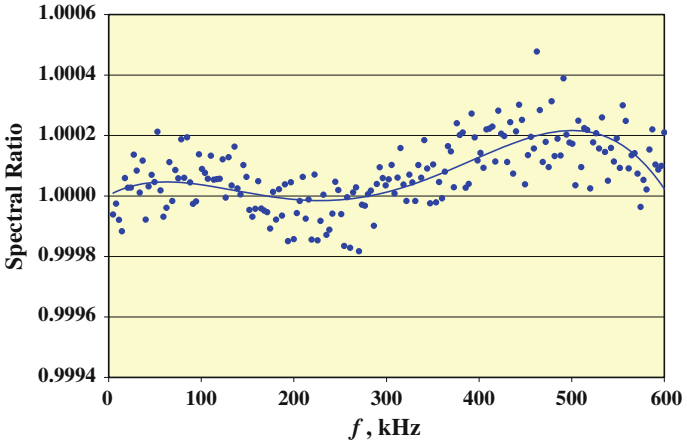

Fig. 4 Ratio of the Jan 505 K spectrum to the Oct 505 K spectrum showing changes in the input network time constants, EMI, and distortion products that took place over the three-month time interval of the experiment. A 4th-order polynomial function may be fit to the data as shown in the *solid curve* to approximate the overall frequency dependence with $a_0 - 1 = 2\ \mu\mathrm{K} \cdot \mathrm{K}^{-1}$

uous time intervals which were never greater then 24 days, and in most cases, less than 2 weeks in length. Other longer-term drift can occur, such as the trend that is observed in the a_4 coefficient in the absolute-mode spectra, but this is complicated by other concurrent changes that may occur in both the EMI and the distortion products. This is most readily observed by forming a relative-ratio spectrum from the Oct 505 and the Jan 505 spectra spanning a three-month time difference. This spectrum is shown in Fig. 4 and exhibits a more complex pattern with either a higher-degree even-order characteristic or 4th-order with significant odd-degree terms. We interpret this as a variable distortion pattern superimposed with slowly variable input-network time constants. Some slow changes in the input networks are to be expected from normal environmental changes such as ambient temperature and humidity. The variable distortion is anomalous, however, primarily originating in the Jan 505 data group. These anomalous changes most likely occurred from transient saturation in certain stages of the amplification chain in response to out-of-band EMI that was observed during the final weeks of the experiment.

When similar relative-mode spectra are formed from absolute-mode spectra taken at the same temperature, but with shorter time differences, the resulting relative-mode ratio spectra appear random, with no apparent structure like that of Fig. 4. Furthermore, the excellent agreement between the two relative-mode ratio spectra, Nov 694/Oct 505 and Dec 692/Jan 505, could not occur under a secular systematic drift since their relative time differences are of the opposite sign. We conclude that, whatever the origin of the long-term drift exhibited in Fig. 4, its influence on the a_0 parameter of the correction models is small, particularly for the relative-ratio spectra which are formed from data separated by <1 month (i.e., Nov 694/Oct 505 and Dec 692/Jan 505). Since we have already made allowances in the uncertainty budget for both EMI and dis-

tortion effects, we therefore do not include any additional uncertainty component for instability.

4.5 QVNS Reference Spectra

The quantized nature of the voltages produced by the QVNS and its wide bandwidth ensure that the uncertainties arising from the QVNS are small. However, there is still potential for errors, and the most significant error contribution comes from undesired non-quantized signals associated with the current sources biasing the QVNS, such as input–output coupling and bias currents driving inductance in the QVNS circuit. These errors, which fortunately have been undetectable thus far, are most significant at higher frequencies, so they would likely be removed through the fitting analysis.

The absolute uncertainty of the local master clock also contributes to the QVNS output uncertainty. The Gaithersburg JNT system uses a 10 MHz oven-stabilized crystal oscillator timebase for the reference clock which synchronizes both the ADCs and the 10 GHz clock for the bit stream generator. The master clock uncertainty is $\sim 0.1\ \mu\mathrm{Hz} \cdot \mathrm{Hz}^{-1}$ which has been verified by comparison with a rubidium frequency standard. The estimated timebase drift is $0.01\ \mu\mathrm{Hz} \cdot \mathrm{Hz}^{-1} \cdot \mathrm{year}^{-1}$ or $0.0025\ \mu\mathrm{Hz} \cdot \mathrm{Hz}^{-1}$ uncertainty in the relative mode over the 90-day duration of the experiment.

4.6 Resistance Measurements

As already discussed in Sect. 2.2 above, we assign a combined measurement uncertainty of $2\ \mu\Omega \cdot \Omega^{-1}$ for the absolute resistance. For the relative-mode spectra, we assign an uncertainty of $1\ \mu\Omega \cdot \Omega^{-1}$ for the resistance ratio $R(694\ \mathrm{K})/R(505\ \mathrm{K})$.

4.7 Spectral Aberrations

Several errors in the fidelity of absolute-mode noise ratio spectra can occur due to limitations in comparing continuous versus discrete spectra. Some of these have been treated by White and Benz [8] and the effects are most noticeable beyond 500 kHz for the type of low-pass filter employed in this work. These effects are currently unresolvable, however, due to the much higher distortion levels present in the ratio spectra of this work.

Other types of spectral aberrations can occur due to digital sampling errors, or aliasing. Aliasing effects are attenuated by the low-pass filter, but in this work we were limited to a single stage with 11 poles, whereas the Boulder JNT system utilizes a total of 22 poles in two separate buffered filter stages. We assume, however, that the only aliasing errors that would matter in the absolute-mode spectral ratio would be those that are different for the R and Q spectra and would be evident through comparison of "Bin" and "Peak"-averaged spectra as described in Sect. 4.3. A $10\ \mu\mathrm{K} \cdot \mathrm{K}^{-1}$ uncertainty estimate for the absolute mode accounts for these effects. We further assume that any such aliasing effects nearly cancel in the relative-mode ratio spectra since the

input network time constants differ by only $R(673\ \mathrm{K}) - R(505)/R(505\ \mathrm{K}) \cong 5.5\,\%$ leaving only a negligible aliasing uncertainty.

It has been shown by Qu et al. [14] that high-frequency distortion (0.6 MHz to 4 MHz, which is visible only around 3 MHz) can alias into the measurement bandwidth. This produced aliased spectral content that contaminated the in-band ($f < 600$ kHz) spectra. This effect was previously incorrectly interpreted as a -80 dBc stop band of the passive filters. We have since determined the actual filter stop band to be ~ -110 dBc and that the effect was actually due to overdriving a buffer amplifier stage, which produced nonlinearities, between the low-pass filter and the ADC. The present results are expected to suffer less from this type of error, because the gain of our buffer amplifier is lower.

4.8 ITS-90

The uncertainties associated with ITS-90 temperatures are shown in Table 7. These include contributions from measurement statistics, calibration, stability, temperature non-uniformity, and resistance ratios. The two SPRTs (serial numbers 1528 and 1548) were in good agreement ($\Delta T_{90} \leq 1$ mK) during the three-month interval of the experiment. The maximum observed change in the WTP values of these two SPRTs was -0.5 mK during a one-year period which included the three-month long period of the experiment.

4.9 Total Combined Uncertainty

The uncertainty budget for the noise measurements is shown in Table 8 along with a summary of the ITS-90 uncertainties and the total combined uncertainties for $\varepsilon_{\mathrm{am}}(505\ \mathrm{K})$ and $\varepsilon_{\mathrm{am}}(693\ \mathrm{K})$ in the absolute mode and $\varepsilon_{\mathrm{rm}}(693\ \mathrm{K})$ in the relative mode. An additional 1.7 $\mu\mathrm{K}\cdot\mathrm{K}^{-1}$ uncertainty contribution from k_{B} is required in the absolute mode, while the uncertainty in K_{J} is only 0.05 $\mu\mathrm{K}\cdot\mathrm{K}^{-1}$. These contributions do not enter into the relative mode uncertainty.

4.10 Determination of Noise Temperatures

The results for the absolute spectra are summarized in Table 9 in terms of $\varepsilon \equiv a_0 - 1 = T/T_{90} - 1$ (i.e., relative to ITS-90) expressed in $\mu\mathrm{K}\cdot\mathrm{K}^{-1}$ and $T - T_{90}$ expressed

Table 7 ITS-90 uncertainties

	505 K (mK)	692 K to 694 K (mK)
Statistics	0.5	3
Non-uniformity	1	3
R-probe immersion	1	2
Resistance ratio	0.25	0.25
Calibration	0.1	0.25
Stability	0.5	3
RSS	1.6	5.6

Table 8 Noise measurement (Type A and Type B) and combined uncertainties for the absolute-mode and relative-mode temperature determinations

	Absolute ($\mu K \cdot K^{-1}$)	Relative ($\mu K \cdot K^{-1}$)	Absolute 693 K (mK)	Absolute 505 K (mK)	Relative 693 K (mK)
Statistics (A)	26	21	18.0	13.1	14.6
Correction model (B)	25	10.0	13.9	10.1	6.9
EMI (B)	14	14	9.7	7.1	9.7
QVNS (B)	0.1	<0.1	0.07	0.05	<0.07
Resistance (B)	2	1.0	1.4	1.0	0.7
Distortion (B)	11	3.7	7.6	5.6	2.5
Spec. aberrations (B)	10		7	5	
Fund. constants (B)	1.7		1.2	0.9	
RSS B	29	18	20	15	12
RSS A + B	39	27	27	20	19
ITS90					
505 K	3.2	–	–	1.6	–
693 K	8.1	9	5.6	–	6.0
AGT correction to 505 K	–	5.9	–	–	4.1
Combined total uncertainty					
505 K	39	–	–	20	–
693 K	40	29	27	–	20

Table 9 Summary of results and combined standard uncertainties of absolute noise temperatures from the absolute ratio spectra of the four data groups based on 3PE model $+a_1$ *a priori* corrections with respect to ITS-90

Data group	$(T - T_{90})/T_{90}(\mu K \cdot K^{-1})$	$T - T_{90}$ (mK)
Oct 505	19 (39)	9.5 (20)
Nov 694	−5 (40)	−3.5 (27)
Dec 692	−2 (40)	−1.4 (27)
Jan 505	8 (39)	3.4 (20)

in mK together with their *combined* standard uncertainties. These results are derived from the 3PE model correction and the *a priori* correction for a_1 in Table 5. The average (Oct 505 and Jan 505) absolute noise temperature relative to the ITS-90 is $\varepsilon_{Sn} = +13(39)\ \mu K \cdot K^{-1}$ which agrees well with the much less uncertain acoustic gas thermometry (AGT) result of $\varepsilon_{Sn} = +21.2(5.9)\ \mu K \cdot K^{-1}$ from Strouse et al. [16]. Alternatively, if our absolute data at 505 K are combined with the AGT temperature for the Sn FP in Eq. 3, a value may be computed for the Boltzmann constant which is $-8(40) \times 10^{-6}$ in relative difference from the current recommended value [17].

The values of $a_0 - 1$ from the relative-mode spectra represent differences in the relative temperature difference or $\varepsilon_{Zn} - \varepsilon_{Sn}$. If the ITS-90 value for the Sn freezing point (505.078 K) was assumed to be thermodynamically correct, then $\varepsilon_{Sn} = 0$

Table 10 Summary of results with respect to ITS-90 and combined standard uncertainties from the relative ratio spectra as corrected to AGT results at 505 K and the 3PA model

Data group combination	T_{90} (K)	$(T - T_{90})/T_{90}(\mu K \cdot K^{-1})$	$T - T_{90}$ (mK)
Nov 694/Oct 505	693.94	5 (29)	3.6 (20)
Dec 692/Jan 505	692.49	6 (29)	4.3 (20)

Table 11 Comparison of recent literature values for $T - T_{90}$ near the Zn FP, in mK

Citation, year	Taubert et al. 2003 [18]	Noulkow et al. 2007 [19]	Noulkow et al. 2007 [19]	Tew et al. 2007 [2]	Labenski et al. 2008 [3]	This work 2010
Method	IRFR 1 μm	IRFR 1.3 μm	IRFR 1.55 μm	RR-JNT	RQ-JNT	RQ-JNT
$T - T_{90}$	41(45)	28(29)	10(34)	−7(31)[a]	+7(30)	+4(18)

IRFR infrared filter radiometry, *RR-JNT* relative resistance-based Johnson noise thermometry, *RQ-JNT* relative quantized voltage-based Johnson noise thermometry

[a] Adjusted by $+10\ \mu K \cdot K^{-1}$ from as-published value due to a statistical offset [6]

and the relative noise temperature for the Zn freezing point would be equivalent to $a_0 - 1$ (i.e., derived from Table 4). In contrast, we make a correction to the ITS-90 using the best available thermodynamic determination of that temperature which is the AGT result from Strouse et al. [16]. This same $+21.2\ \mu K \cdot K^{-1}$ correction was used in our 2008 Zn FP determination. The results for the as-corrected relative-mode spectra are summarized in Table 10 together with combined standard uncertainties using the two statistically independent combinations of data groups: Nov 694/Oct 505 and Dec 692/Jan 505. The absolute and relative mode results at 692 K and 694 K are self-consistent. When the two data group combinations for 692 K and 694 K are combined, the result is $\varepsilon_{Zn} = 5.7(25)\ \mu K \cdot K^{-1}$ or $T - T_{90} = +4(18)$ mK.

5 Conclusions

We have replicated a series of noise temperature measurements which re-determine the noise temperature for the zinc freezing point relative to that of the Sn freezing point. Our new relative mode value for the Zn freezing point is $\varepsilon_{Zn}(693\ K) = +6(25)\ \mu K \cdot K^{-1}$ or $T - T_{90} = +4(18)$ mK. In addition we report, for the first time in this range, absolute noise temperature results of $T - T_{90} = +6.7(20)$ mK for the Sn FP and $T - T_{90} = -2.5(27)$ mK for the Zn FP. Comparisons of these results to our past JNT results and with other recent literature values from infrared (IR) filter radiometry are shown in Table 11. The results from this and our 2008 quantized voltage-based JNT determinations are in good agreement with the IR filter radiometry.

Further work is underway to improve the electronics to reduce distortion. New measurements are planned to extend the range of temperatures above 693 K.

Acknowledgments We gratefully acknowledge the important work of Jifeng Qu while serving as a guest researcher at NIST Boulder, enabling technical advances which benefited this work in Gaithersburg. We also gratefully acknowledge Charlie Burroughs for chip packaging and Sae Woo Nam and John Martinis for their important contributions in the earliest development stages of NIST JNT programs. Special thanks

go to Greg Strouse for SPRT calibrations. We received helpful comments from Richard Steiner and Mike Moldover of NIST.

References

1. S.P. Benz, J.F. Qu, H. Rogalla, D.R. White, P.D. Dresselhaus, W.L. Tew, S.W. Nam, IEEE Trans. Instrum. Meas. **58**, 884 (2009)
2. W.L. Tew, J.R. Labenski, S.W. Nam, S.P. Benz, P.D. Dresselhaus, C.J. Burroughs, Int. J. Thermophys. **28**, 629 (2007)
3. J.R. Labenski, W.L. Tew, S.P. Benz, S.W. Nam, P. Dresselhaus, Int. J. Thermophys. **29**, 1 (2008)
4. S.P. Benz, J.M. Martinis, P.D. Dresselhaus, S.W. Nam, IEEE Trans. Instrum. Meas. **52**, 545 (2003)
5. S.P. Benz, D.R. White, J.F. Qu, H. Rogalla, W.L. Tew, C.R. Phys. **10**, 849 (2009)
6. D.R. White, S.P. Benz, J.R. Labenski, S.W. Nam, J.F. Qu, H. Rogalla, W.L. Tew, Metrologia **45**, 395 (2008)
7. S.P. Benz, J.M. Martinis, S.W. Nam, W.L. Tew, D.R. White, in *Proceedings of TEMPMEKO 2001, 8th International Symposium on Temperature and Thermal Measurements in Industry and Science*, ed. by B. Fellmuth, J. Seidel, G. Scholz (VDE Verlag, Berlin, 2002), pp. 37–44
8. D.R. White, S.P. Benz, Metrologia **45**, 93 (2008)
9. J.R. Labenski, W.L. Tew, S.W. Nam, S.P. Benz, P.D. Dresselhaus, C.J. Burroughs, IEEE Trans. Instrum. Meas. **56**, 481 (2007)
10. D.R. White, E. Zimmermann, Metrologia **37**, 11 (2000)
11. S.W. Nam, S.P. Benz, J.M. Martinis, P. Dresselhaus, W.L. Tew, D.R. White, in *Temperature: Its Measurement and Control in Science and Industry*, vol. 7, ed. by D.C. Ripple (AIP, Chicago, 2003), pp. 37–42
12. B.W Mangum, G.T. Furukawa, *Guidelines for Realizing the International Temperature Scale of 1990 (ITS-90)* (U.S. Department of Commerce, National Institute of Standards and Technology, Gaithersburg, 1990)
13. S.P. Benz, C.A. Hamilton, Appl. Phys. Lett. **68**, 3171 (1996)
14. J.F. Qu, S.P. Benz, H. Rogalla, D.R. White, Metrologia **46**, 512 (2009)
15. S.W. Nam, S.P. Benz, P.D. Dresselhaus, W.L. Tew, D.R. White, J.M. Martinis, IEEE Trans. Instrum. Meas. **52**, 550 (2003)
16. G.F. Strouse, D.R. Defibaugh, M.R. Moldover, and D.C. Ripple, in *Temperature: Its Measurement and Control in Science and Industry*, vol. 7, ed. by D.C. Ripple (AIP, Chicago, 2003), pp. 31–36
17. P.J. Mohr, B.N. Taylor, D.B. Newell, Rev. Mod. Phys. **80**, 633 (2008)
18. D.R. Taubert, J. Hartmann, J. Hollandt, J. Fischer, in *Temperature: Its Measurement and Control in Science and Industry*, vol. 7, ed. by D.C. Ripple (AIP, Chicago, 2003), pp. 7–12
19. N. Noulkow, R. Taubert, P. Meindl, J. Hollandt, Int. J. Thermophys. **30**, 131 (2009)